A Geometrical Optics Model of Three Dimensional Scattering From a Rough Surface Over a Planar Surface

Nicolas Pinel, *Member, IEEE*, Joel T. Johnson, *Fellow, IEEE*, and Christophe Bourlier, *Associate Member, IEEE*

***Abstract*—An analytical method is described for predicting the bistatic normalized radar cross section of a rough homogeneous layer made up of a rough surface over a flat surface. The model is based on iteration of the Kirchhoff approximation to calculate the fields scattered by the rough layer, and is reduced to the high-frequency limit in order to obtain numerical results rapidly. The shadowing effect, significant for larger incidence or scattering angles, is taken into account through the use of shadowing functions. The model is applicable for moderate to large upper surface roughnesses having small to moderate slopes, and for both lossless and lossy inner media. It was validated for a two-dimensional problem (with 1D surfaces) in a preceding contribution. Here, the extension of the model to 2D surfaces is developed, and results are presented to validate the asymptotic model by comparison with a numerical reference method.**

***Index Terms*—Electromagnetic scattering by rough surfaces, multilayered media, multistatic scattering, physical optics.**

I. Introduction

SCATTERING from dielectric homogeneous layers has many applications in remote sensing, including the sensing of ocean ice, sand cover of arid regions, or oil slicks on the ocean, as well as in optics, including optical studies of thin films/coated surfaces and analysis of antireflection coatings. The use of asymptotic models can be very useful to predict the scattered signal of such systems, as such models provide fast numerical results compared to "exact" numerical methods (for instance, see [1]–[3] and references therein), while retaining accuracy for specific classes of surfaces.

Many asymptotic models of electromagnetic scattering from a single rough interface have been developed over the last years. By contrast, few asymptotic models have been developed for rough layers separating homogeneous media, see mainly [4]–[9]. Most of the available asymptotic models for rough layers are difficult to implement numerically and demand extensive computing time. To our knowledge, the specific case of rough layers with rms heights that may be large compared to the electromagnetic wavelength (while retaining moderate slopes) has not been treated before, and is the subject of this paper. The aim of this paper is to extend the Kirchhoff approximation to the case of a rough layer (with a rough upper interface and a perfectly flat lower interface) and to obtain a formulation of the bistatic normalized radar cross section (NRCS) in the high-frequency limit. The model has been described in recent publications [10], [11] for one-dimensional (1D) rough layers, in which the surface shadowing effect is taken into account [12], [13]. Here, the extension of the model to two-dimensional (2D) rough layers is developed in order to include general three-dimensional (3D) problems and to study scattering in cross-polarizations. Numerical results are presented and compared with a reference numerical method to validate the model.

Manuscript received May 07, 2008; revised October 07, 2008. Current version published March 20, 2009.

N. Pinel and C. Bourlier are with the Radar Team of Institut de Recherche en Electrotechnique et Electronique de Nantes Atlantique (IREENA) Laboratory, Université Nantes Angers Le Mans, Polytech'Nantes, 44306 Nantes Cedex 3, France (e-mail: nicolas.pinel@univ-nantes.fr; christophe.bourlier@univ-nantes.fr).

J. T. Johnson is with the Department of Electrical and Computer Engineering and the ElectroScience Laboratory, The Ohio State University, Columbus, OH 43210 USA (e-mail: johnson@ece.osu.edu).

Color versions of one or more of the figures in this paper are available online at http://ieeexplore.ieee.org.

Digital Object Identifier 10.1109/TAP.2008.2011252

II. Calculation of the Scattered Fields Derived With the KA and the MSP

A. Problem Presentation

The studied system (see Fig. 1) is composed of a rough layer (with a rough upper interface Σ_A and a perfectly flat lower interface Σ_B), separating homogeneous media Ω_α, with $\alpha = \{1,2,3\}$. The three media Ω_α, with relative permittivity $\epsilon_{r\alpha}$, are assumed to be non magnetic (relative permeability $\mu_r = 1$). Let $\mathbf{E_i}$ be the incident field of polarization $\hat{\mathbf{e}}_\mathbf{i}$ inside the medium Ω_1 in the direction $\hat{\mathbf{K}}_\mathbf{i} = (k_{ix}, k_{iy}, k_{iz})/|k_1| = (\hat{k}_{ix}, \hat{k}_{iy}, \hat{k}_{iz})$ (the elevation angle, with respect to the vertical axis $\hat{\mathbf{z}}$, being θ_i, and the azimuth angle, with respect to the axis $\hat{\mathbf{x}}$, being ϕ_i). The incident field on the upper surface Σ_A at the point A_1 is given by $\mathbf{E_i}(\mathbf{R_{A_1}}) = E_0 e^{ik_1 \hat{\mathbf{K}}_\mathbf{i}\cdot\mathbf{R_{A_1}}} \hat{\mathbf{e}}_\mathbf{i}$ (the term $e^{-i\omega t}$ is omitted) where $\mathbf{R_{A_1}} = x_{A_1}\hat{\mathbf{x}} + y_{A_1}\hat{\mathbf{y}} + z_{A_1}\hat{\mathbf{z}}$, with x_{A_1} and y_{A_1} the abscissa, and z_{A_1} the elevation of the point A_1. k_1 is the wave number inside Ω_1 (relative permittivity ϵ_{r1}).

The field transmitted into the intermediate medium Ω_2 along the direction $\hat{\mathbf{K}}_\mathbf{m1}$ is reflected by the flat lower interface at the point B_1 into the specular direction $\hat{\mathbf{K}}_\mathbf{p1}$, and then reflected by the upper surface at the point A_2, and so on. Thus, multiple reflections of the field inside Ω_2 occur, and this system can be seen as a rough dielectric waveguide. The first two scattered fields in reflection, $\mathbf{E_{r,1}}$ and $\mathbf{E_{r,2}}$, are treated in detail in this paper; higher orders can be expressed at any order in reflection in a similar manner to that described here. $\mathbf{E_{r,1}}, \mathbf{E_{r,2}}$ are observed

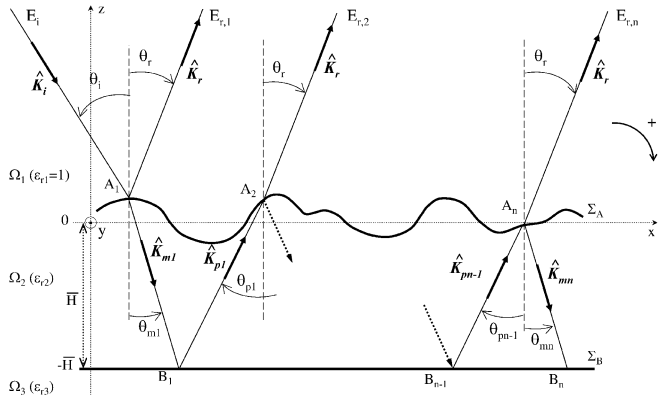

Fig. 1. Multiple scattering from a rough layer with a rough upper interface and a flat lower interface, represented in the plane $(\hat{\mathbf{x}}, \hat{\mathbf{z}})$. The points on the upper surface Σ_A are denoted as $\{A_1, A_2, \ldots, A_n\}$, whereas the points on the lower surface Σ_B are denoted as $\{B_1, B_2, \ldots, B_{n-1}\}$. θ_i is the elevation incidence angle, and θ_r is the elevation scattering angle in reflection, measured with respect to the vertical axis $\hat{\mathbf{z}}$. The positive sense is defined as clockwise.

in the direction $\hat{\mathbf{K}}_\mathbf{r} = (k_{rx}, k_{ry}, k_{rz})/|k_1| = (\hat{k}_{rx}, \hat{k}_{ry}, \hat{k}_{rz})$. The unit wave vectors $\hat{\mathbf{K}}_\mathbf{i}, \hat{\mathbf{K}}_\mathbf{r}, \hat{\mathbf{K}}_\mathbf{m1}, \hat{\mathbf{K}}_\mathbf{p1}$ are defined by

$$\hat{\mathbf{K}}_\mathbf{i} = (\sin\theta_i \cos\phi_i,\ \sin\theta_i \sin\phi_i,\ -\cos\theta_i) \tag{1a}$$

$$\hat{\mathbf{K}}_\mathbf{r} = (\sin\theta_r \cos\phi_r,\ \sin\theta_r \sin\phi_r,\ +\cos\theta_r) \tag{1b}$$

$$\hat{\mathbf{K}}_\mathbf{m1} = (\sin\theta_{m1} \cos\phi_{m1}, \sin\theta_{m1} \sin\phi_{m1}, -\cos\theta_{m1}) \tag{1c}$$

$$\hat{\mathbf{K}}_\mathbf{p1} = (\sin\theta_{p1} \cos\phi_{p1},\ \sin\theta_{p1} \sin\phi_{p1},\ +\cos\theta_{p1}). \tag{1d}$$

In order to calculate the fields $\mathbf{E_{r,1}}$ and $\mathbf{E_{r,2}}$, the Kirchhoff approximation (KA) (which is sometimes also called physical optics approximation, or tangent plane approximation) is used for the (upper) rough interface, and the Weyl representation of the Green's function is used to describe the propagation from one scattering point to another. More precisely, the KA is iterated for each scattering inside the rough layer, i.e. on the interaction among interfaces (and not for multiple scattering from the rough interface). The field at any point of the (upper) rough surface can then be approximated by the field that would be present on its infinite tangent plane. Thus, the Snell-Descartes laws and the Fresnel coefficients can be applied locally, at any point of the (upper) rough surface. This approach should be valid at moderate incidence angles and for interfaces whose radii of curvature are much larger than the incident wavelength λ. Moreover, by neglecting the multiple scattering from the same interface effect, it should be valid for moderate rms slopes and for near-specular scattering geometries.

The formulation is further simplified by applying the method of stationary phase (MSP) for each scattering point inside the rough layer. The MSP is an approximation of the KA that assumes that the major contribution of the scattered field comes from regions of the rough surface in the vicinity of the (stationary phase) specular points of the rough surface, whose direction is given by the local normal to the surface and the incidence angle. This approximation is valid for moderately rough to very rough interfaces [14]. Using these two approximations, simplified expressions of $\mathbf{E_{r,1}}$ and $\mathbf{E_{r,2}}$ can be obtained: in the case of 1D surfaces, with 1 integration for $\mathbf{E_{r,1}}$, and 3 fold integrations for $\mathbf{E_{r,2}}$ [10]. Here, for the case of 2D surfaces, one will see that the number of numerical integrations is doubled.

B. Fields Scattered by the Rough Layer

The fields scattered in reflection $\mathbf{E_{r,1}}$ inside Ω_1 and transmission $\mathbf{E_{m1}}$ inside Ω_2 by the upper interface Σ_A at the point A_1 are obtained from the Kirchhoff-Helmholtz integral equations [15], [16]. Under the KA, these expressions can be written as

$$\begin{aligned}\mathbf{E_{r,1}}(\mathbf{R}) = &+ 2ik_1(\bar{\mathbf{I}} - \hat{\mathbf{K}}_\mathbf{r}\hat{\mathbf{K}}_\mathbf{r}) \cdot \int\int dx_{A_1} dy_{A_1} \\ &G_1(\mathbf{R_{A_1}}, \mathbf{R})\, \mathbf{F_r}(\gamma_{A_1,x}, \gamma_{A_1,y}) \\ &\times E_i(\mathbf{R_{A_1}})\, \Xi_r(\mathbf{R_{A_1}})\end{aligned} \tag{2a}$$

$$\begin{aligned}\mathbf{E_{m1}}(\mathbf{R}) = &- 2ik_2(\bar{\mathbf{I}} - \hat{\mathbf{K}}_\mathbf{m1}\hat{\mathbf{K}}_\mathbf{m1}) \cdot \int\int dx_{A_1} dy_{A_1} \\ &G_2(\mathbf{R_{A_1}}, \mathbf{R})\, \mathbf{F_{m1}}(\gamma_{A_1,x}, \gamma_{A_1,y}) \\ &\times E_i(\mathbf{R_{A_1}})\, \Xi_t(\mathbf{R_{A_1}})\end{aligned} \tag{2b}$$

where Ξ_r and Ξ_t are the illumination function in reflection and transmission, respectively (i.e., with $\Xi_{r,t} = 1$ if the rays emanating from both the incident and the scattered waves do not cross the surface except from considered surface point A_1, corresponding to $\mathbf{R_{A_1}}$; $\Xi_{r,t} = 0$ otherwise); $x_{A_1} \in [-L_{Ax}/2; +L_{Ax}/2]$ and $y_{A_1} \in [-L_{Ay}/2; +L_{Ay}/2]$ (the surface lengths L_{Ax} and L_{Ay} are assumed to be much greater than their correlation length L_{cAx}, L_{cAy}, respectively, and than the wavelength λ). In the above equations, the Weyl representation of the Green's function is used to describe the propagation of the scattered wave from a point $\mathbf{R_{A_n}}$ (with $n = 1$ here) of the upper interface to the point $\mathbf{R}$ of considered medium Ω_α. Its expression is given by [8], [17], [18]

$$G_\alpha(\mathbf{R}, \mathbf{R_{A_n}}) = \frac{i}{2} \int \frac{d\mathbf{k}}{(2\pi)^2} \frac{e^{i\mathbf{k}\cdot(\mathbf{r}-\mathbf{r_{A_n}}) + if(\mathbf{k})|z-\zeta_{A_n}|}}{f(\mathbf{k})} \tag{3}$$

where $\mathbf{k} = k_x\hat{\mathbf{x}} + k_y\hat{\mathbf{y}}$ (k_x and k_y ranging $]-\infty; +\infty[$) and $\mathbf{r} = x\hat{\mathbf{x}} + y\hat{\mathbf{y}}$, with

$$f(\mathbf{k}) = \begin{cases} \sqrt{k_\alpha^2 - \|\mathbf{k}\|^2} & \text{if } k_\alpha^2 \geq \|\mathbf{k}\|^2 \\ i\sqrt{\|\mathbf{k}\|^2 - k_\alpha^2} & \text{if } k_\alpha^2 < \|\mathbf{k}\|^2. \end{cases} \tag{4}$$

If the point $\mathbf{R}$ is in the far-field zone of the surface Σ_A, corresponding to inequality $\|\mathbf{R}\| \gg \|\mathbf{R_{A_n}}\|$, the Green's function can be approximated by

$$G_\alpha(\mathbf{R}, \mathbf{R_{A_n}}) \simeq \frac{\exp\left[i\left(k_\alpha R - \mathbf{K_s}\cdot\mathbf{R_{A_n}}\right)\right]}{4\pi R} \tag{5}$$

with $\mathbf{K_s} = \mathbf{K_r}$ for $\alpha = 1$.

Substituting the expression of the far-field Green's function (5) in (2a), in the far-field zone the first-order scattered field $\mathbf{E^\infty_{r,1}}(\mathbf{R})$ can be expressed under the MSP by

$$\begin{aligned}\mathbf{E^\infty_{r,1}}(\mathbf{R}) = &+ \frac{ik_1 E_0 e^{ik_1 R}}{2\pi R}(\bar{\mathbf{I}} - \hat{\mathbf{K}}_\mathbf{r}\hat{\mathbf{K}}_\mathbf{r}) \cdot \mathbf{F_r}\left(\gamma^\mathbf{0}_\mathbf{A_1}\right) \\ &\times \int d\mathbf{r_{A_1}}\, e^{i(\mathbf{K_i}-\mathbf{K_r})\cdot\mathbf{R_{A_1}}}\, \Xi_r(\mathbf{R_{A_1}})\end{aligned} \tag{6}$$

where $\int d\mathbf{r_{A_1}} \equiv \int\int dx_{A_1} dy_{A_1}$, and $\mathbf{F_r}(\gamma^{\mathbf{0}}_{\mathbf{A_1}})$ is given by [19, Eq. (2.1.55a)], with $\gamma^{\mathbf{0}}_{\mathbf{A_1}} = (\gamma^0_{A_1,x}, \gamma^0_{A_1,y})$ given by

$$\gamma^0_{A_1,x} \equiv \gamma^{0(r)}_{A_1,x} = -(k_{rx} - k_{ix})/(k_{rz} - k_{iz}) \tag{7}$$

$$\gamma^0_{A_1,y} \equiv \gamma^{0(r)}_{A_1,y} = -(k_{ry} - k_{iy})/(k_{rz} - k_{iz}). \tag{8}$$

Similarly, the higher-order scattered fields ($\mathbf{E_{r,2}}, \mathbf{E_{r,3}}$, etc.) are obtained from (2b) by first using the Weyl representation of the Green function which describes the propagation of the wave from $\mathbf{R_{A_n}}$ to the point $\mathbf{R_{A_{n+1}}}$ of the upper interface Σ_A, after reflection onto the flat lower interface Σ_B at the point B_n of elevation $z_B = -\bar{H}$. It is given by [17], [20]

$$G_{2,r}\left(\mathbf{R_{A_{n+1}}}, \mathbf{R_{A_n}}\right) = \frac{i}{2} \times \int \frac{d\mathbf{k}}{(2\pi)^2} r(\mathbf{k}) \frac{e^{i\mathbf{k}\cdot\left(\mathbf{r_{A_{n+1}}} - \mathbf{r_{A_n}}\right) + if(\mathbf{k})\left(\zeta_{A_{n+1}} - \zeta_{A_n} - 2z_B\right)}}{f(\mathbf{k})} \tag{9}$$

with $r(\mathbf{k})$ the Fresnel reflection coefficient of the lower interface.

Then, the scattering in reflection and transmission at the point A_2 is described by the Kirchhoff-Helmholtz integral equation under the KA, expressed in reflection $\mathbf{E_{m2}}$ inside Ω_2 and in transmission $\mathbf{E_{r,2}}$ inside Ω_3 by

$$\mathbf{E_{m2}}(\mathbf{R}) = +2ik_2(\bar{\mathbf{I}} - \hat{\mathbf{K}}_{\mathbf{m2}}\hat{\mathbf{K}}_{\mathbf{m2}}) \cdot \int\int dx_{A_2} dy_{A_2} G_2\left(\mathbf{R_{A_2}}, \mathbf{R}\right) \mathbf{F_{m2}}\left(\gamma_{\mathbf{A_2}}\right) \times E_{p1}\left(\mathbf{R_{A_2}}\right) \Xi_r\left(\mathbf{R_{A_2}}\right) \tag{10a}$$

$$\mathbf{E_{r,2}}(\mathbf{R}) = -2ik_1(\bar{\mathbf{I}} - \hat{\mathbf{K}}_{\mathbf{r}}\hat{\mathbf{K}}_{\mathbf{r}}) \cdot \int\int dx_{A_2} dy_{A_2} G_1\left(\mathbf{R_{A_2}}, \mathbf{R}\right) \mathbf{F_t}\left(\gamma_{\mathbf{A_2}}\right) \times E_{p1}\left(\mathbf{R_{A_2}}\right) \Xi_t\left(\mathbf{R_{A_2}}\right) \tag{10b}$$

respectively, with $x_{A_2} \in [-L_{Ax}/2; +L_{Ax}/2]$ and $y_{A_2} \in [-L_{Ay}/2; +L_{Ay}/2]$, and the field inside Ω_2 incident on the upper interface at the point A_2, $E_{p1}(\mathbf{R_{A_2}})$, being obtained from the relation

$$E_{p1}\left(\mathbf{R_{A_2}}\right) = G_{2,r}\left(\mathbf{R_{A_2}}, \mathbf{R_{A_1}}\right) E_{m1}\left(\mathbf{R_{A_1}}\right). \tag{11}$$

Thus, under the MSP and by neglecting the evanescent wave contribution, by using the far-field Green function (5) at the point $A_n = A_2$, $\mathbf{E^{\infty}_{r,2}}$ is expressed by

$$\frac{\mathbf{E^{\infty}_{r,2}}(\mathbf{R})}{E_0} = \frac{ik_1k_2e^{ik_1R}}{(2\pi)^3R} \int \frac{d\mathbf{k_{m1}}}{-k_{m1z}} d\mathbf{r_{A_1}} d\mathbf{r_{A_2}} \cdot \mathbf{F_{m1}}\left(\gamma^{\mathbf{0}}_{\mathbf{A_1}}\right) \times \bar{r}_{23}(\theta_{m1}) \times \mathbf{F_r}\left(\gamma^{\mathbf{0}}_{\mathbf{A_2}}\right) \cdot e^{i\left(\mathbf{K_i}\cdot\mathbf{R_{A_1}} + \mathbf{K_{m1}}\cdot\mathbf{R_{A_1B_1}} + \mathbf{K_{p1}}\cdot\mathbf{R_{B_1A_2}} - \mathbf{K_r}\cdot\mathbf{R_{A_2}}\right)} \cdot \delta(\hat{\mathbf{k}}_{\mathbf{p1}} - \hat{\mathbf{k}}_{\mathbf{m1}}) \Xi_t\left(\mathbf{R_{A_1}}\right) \cdot \Xi_r\left(\mathbf{R_{B_1}}\right) \Xi_t\left(\mathbf{R_{A_2}}\right) \tag{12}$$

with $\mathbf{R_{B_1A_2}} = \mathbf{R_{A_2}} - \mathbf{R_{B_1}}$. The calculation of $\mathbf{E^{\infty}_{r,2}}$ then implies 2×3 fold numerical integrations.

By using the same principle for the higher orders, i.e. by iterating the KA at each scattering point among interfaces, and using the MSP, it is possible to obtain the expressions of the scattered fields in reflection $\mathbf{E^{\infty}_{r,n}}$ at any order $n \in \mathbb{N}^*$. Nevertheless, their expression is long and is consequently not given here.

III. NRCS in the High-Frequency Limit

As for 1D surfaces, the nth order total power $P^{tot}_{r,n} = \langle |E^{tot}_{r,n}|^2 \rangle / 2\eta_1$ scattered by the rough layer is given by equation (14) of [10], and the nth order incoherent total power $P^{tot,inc}_{r,n}$ is given by $P^{tot,inc}_{r,n} = [\langle |E^{tot}_{r,n}|^2 \rangle - |\langle E^{tot}_{r,n} \rangle|^2]/2\eta_1$, with η_1 the wave impedance inside Ω_1.

In order to determine the NRCS in the high-frequency limit, the geometric optics approximation (GOA) is applied on the (upper) rough surface in order to simplify the calculation. Valid for very rough surfaces, it assumes that the main contribution to the power scattered by the rough surface Σ_A comes from closely-located correlated surface points M and M'. Moreover, the height difference $\zeta_M - \zeta_{M'}$ can be expressed by the approximate expression $\gamma_{M,x}(x_M - x_{M'}) + \gamma_{M,y}(y_M - y_{M'})$, with $\gamma_{\mathbf{M}} = (\gamma_{M,x}, \gamma_{M,y})$ the rough surface slope at the point M.

Then, the incoherent total NRCS (equal to the total NRCS $\sigma^{tot}_{r,n}$ under the GOA) of a 2D target (for a 3D problem) can be determined more easily. It is given by

$$\sigma^{tot}_{r,n}(\mathbf{K_r}, \mathbf{K_i}) = 2\eta_1 \frac{R^2 P^{tot}_{r,n}}{L_{Ax} L_{Ay} \cos\theta_i |E_i|^2} \tag{13}$$

where R is the distance of the target, and L_{Ax}, L_{Ay} the upper surface length along direction $\hat{\mathbf{x}}$ and $\hat{\mathbf{y}}$, respectively. In the above equation, for cases $n = \{1, 2\}$, one has the relations

$$P^{tot}_{r,1} = p_{r,1} \text{ and } P^{tot}_{r,2} = p_{r,1} + p_{r,2} \tag{14}$$

with

$$\begin{cases} p_{r,1} = \frac{1}{2\eta_1} \langle |E_{r,1}|^2 \rangle \\ p_{r,2} = \frac{1}{2\eta_1} \left[\langle |E_{r,2}|^2 \rangle + 2\Re e \left(\langle E_{r,1} E^*_{r,2} \rangle \right) \right]. \end{cases} \tag{15}$$

A NRCS corresponding to the contribution of each scattered power can then be defined. Thus, for $n = 1$, $\sigma_{r,1}$ corresponds to the contribution from $p_{r,1}$. For $n = 2$, $\sigma_{r,1}$ corresponds to the contribution from $p_{r,1}$ and $\sigma_{r,2}$ to the contribution from $p_{r,2}$. Under the GOA and with shadowing effect, one can show that the interference term $\langle E_{r,1} E^*_{r,2} \rangle$ equals zero, which is in agreement with the latter approximation. In this model, the shadowing and masking effects in reflection [12] and in transmission [13] are taken into account. Indeed, for low grazing incidence and/or scattering angles, a part of the (upper) rough surface is not illuminated by the local incident wave and/or not seen by the local scattered wave. This phenomenon must be taken into account in order not to overestimate the NRCS.

A. Expressions of the First Three Contributions

The first-order NRCS in reflection $\bar{\sigma}_{r,1}(\mathbf{K_r}, \mathbf{K_i})$ corresponds to the NRCS in reflection from a single rough interface. Under the KA and the MSP, and reduced to the GOA, it is well-known [8], [19] that the NRCS can be expressed by

$$\bar{\sigma}_{r,1}(\mathbf{K_r}, \mathbf{K_i}) = \frac{1}{\cos\theta_i} \left| \bar{F}_r(\mathbf{K_r}, \mathbf{K_i}) \right|^2 \times \frac{p_s\left(\gamma^{\mathbf{0(r)}}_{\mathbf{A_1}}\right)}{|\hat{k}_{rz} - \hat{k}_{iz}|^2} S_{11}\left(\mathbf{K_i}, \mathbf{K_r} | \gamma^{\mathbf{0(r)}}_{\mathbf{A_1}}\right) \tag{16}$$

with $\bar{F}_r(\mathbf{K_i},\mathbf{K_r}) = \hat{\mathbf{a}}_\mathbf{r}\cdot\mathbf{F_b}(\gamma_{\mathbf{A_1}}^{\mathbf{0(r)}})$ being a 2×2 matrix which depends on the polarizations of the incident and the scattered waves, and $S_{11}(\mathbf{K_i},\mathbf{K_r}|\gamma_{\mathbf{A_1}}^{\mathbf{0(r)}})$ given by

$$S_{11} = \begin{cases} \frac{1}{1+\Lambda(\hat{\mathbf{K}}_\mathbf{r})} & \text{if } \{\phi_r = \phi_i+\pi, \theta_r \geq \theta_i\} \\ \frac{1}{1+\Lambda(\hat{\mathbf{K}}_\mathbf{i})} & \text{if } \{\phi_r = \phi_i+\pi, \theta_r < \theta_i\} \\ \frac{1}{1+\Lambda(\hat{\mathbf{K}}_\mathbf{i})+\Lambda(\hat{\mathbf{K}}_\mathbf{r})} & \text{if } \{\phi_r \neq \phi_i+\pi\}. \end{cases} \quad (17)$$

For the second-order contribution, the principle is the same as for 1D surfaces (see [10, Sec. 3.1.1]). Extending the method from 1D surfaces to 2D surfaces does not raise any major problem in the calculation. However, this is true only for the coincidental case. The anti-coincidental case, which may contribute around the backscattering direction, was rather hard to quantify for 1D surfaces. It is then complex to quantify for 2D surfaces. Thus, in this paper we will choose configurations for which this contribution (which may occur only around the backscattering direction) can be neglected: the condition of its contribution is given by [11, Eq. (36)]. Thus, the second-order NRCS $\sigma_{r,2}$ can be written as

$$\begin{aligned}\bar{\sigma}_{r,2}(\mathbf{K_r},\mathbf{K_i}) &= \frac{1}{\cos\theta_i}\int \sin\theta_{m1}d\theta_{m1}d\phi_{m1}\left|\bar{F}_{t,12}(\mathbf{K_i},\mathbf{K_{m1}})\times\bar{r}_{23}(\theta_{m1})\right. \\ &\quad \left.\times\bar{F}_{t,21}(\mathbf{K_{p1}},\mathbf{K_r})\right|^2 \\ &\quad \cdot\frac{p_s\left(\gamma_{\mathbf{A_1}}^{\mathbf{0(t)}}\right)}{\left|\hat{k}_{m1z}-\frac{k_1}{k_2}\hat{k}_{iz}\right|^2}S_{12}\left(\mathbf{K_i},\mathbf{K_{m1}}|\gamma_{\mathbf{A_1}}^{\mathbf{0(t)}}\right) \\ &\quad \cdot\frac{p_s\left(\gamma_{\mathbf{A_2}}^{\mathbf{0(t)}}\right)}{\left|\hat{k}_{rz}-\frac{k_2}{k_1}\hat{k}_{p1z}\right|^2}S_{21}\left(\mathbf{K_{p1}},\mathbf{K_r}|\gamma_{\mathbf{A_2}}^{\mathbf{0(t)}}\right). \end{aligned} \quad (18)$$

with $\gamma_{\mathbf{A_1}}^{\mathbf{0(t)}} = (\gamma_{A_1,x}^{0(t)},\gamma_{A_1,y}^{0(t)})$ and $\gamma_{\mathbf{A_2}}^{\mathbf{0(t)}} = (\gamma_{A_2,x}^{0(t)},\gamma_{A_2,y}^{0(t)})$ given by

$$\gamma_{A_1,x,y}^{0(t)} = -(k_{m1x,y}-k_{ix,y})/(k_{m1z}-k_{iz}) \quad (19)$$

$$\gamma_{A_2,x,y}^{0(t)} = -(k_{rx,y}-k_{p1x,y})/(k_{rz}-k_{p1z}). \quad (20)$$

The bistatic shadowing functions in transmission are given by $S_{12}(\mathbf{K_i},\mathbf{K_{m1}}|\gamma_{\mathbf{A_1}}^{\mathbf{0(t)}}) = B[1+\Lambda(\mathbf{K_i}),1+\Lambda(\mathbf{K_{m1}})]$, and $S_{21}(\mathbf{K_{p1}},\mathbf{K_r}|\gamma_{\mathbf{A_2}}^{\mathbf{0(t)}}) = B[1+\Lambda(\mathbf{K_{p1}}),1+\Lambda(\mathbf{K_r})]$, where B is the Beta function (also called the Eulerian integral of the first kind). The second-order NRCS $\bar{\sigma}_{r,2}$ is expressed in the form of a square matrix of dimension 2, in which each term depends on the polarization of the incident and the scattered waves. The general polarization term $\bar{F}_{s,\alpha\beta}(\mathbf{K_1},\mathbf{K_s})$ being also a matrix, the NRCS cannot rigorously be split up into a product of elementary NRCSs as for the 2D case (with 1D surfaces), corresponding to each scattering point inside the dielectric waveguide. As a general rule, $\bar{\sigma}_{r,2}$ and $\bar{F}_{s,\alpha\beta}(\mathbf{K_1},\mathbf{K_s})$ can be expressed as

$$\bar{\sigma}_{r,2} = \begin{bmatrix} \sigma_{h_rh_i}^{r,2}(\mathbf{K_r},\mathbf{K_i}) & \sigma_{v_rh_i}^{r,2}(\mathbf{K_r},\mathbf{K_i}) \\ \sigma_{h_rv_i}^{r,2}(\mathbf{K_r},\mathbf{K_i}) & \sigma_{v_rv_i}^{r,2}(\mathbf{K_r},\mathbf{K_i}) \end{bmatrix} \quad (21)$$

$$\bar{F}_{s,\alpha\beta}(\mathbf{K_1},\mathbf{K_s}) = \begin{bmatrix} F_{h_sh_1}(\mathbf{K_1},\mathbf{K_s}) & F_{v_sh_1}(\mathbf{K_1},\mathbf{K_s}) \\ F_{h_sv_1}(\mathbf{K_1},\mathbf{K_s}) & F_{v_sv_1}(\mathbf{K_1},\mathbf{K_s}) \end{bmatrix} \quad (22)$$

where the first subscript in the terms inside the matrix represents the polarization of the scattered wave, and the second subscript the polarization of the incident wave. The general polarization term in reflection (for $s\equiv r$, implying $\mathbf{K_s}=\mathbf{K_2}$) $F_{r,\alpha\beta}(\mathbf{K_1},\mathbf{K_2}) = F_r(\mathbf{K_1},\mathbf{K_2})$ is defined by

$$\begin{aligned} F_r(\mathbf{K_1},\mathbf{K_2}) &= \frac{\|\hat{\mathbf{K}}_\mathbf{2}-\hat{\mathbf{K}}_\mathbf{1}\|^2}{\|\hat{\mathbf{K}}_\mathbf{1}\wedge\hat{\mathbf{K}}_\mathbf{2}\|^2|\hat{k}_{2z}-\hat{k}_{1z}|} \\ &\quad\times\left\{\frac{r_h(\chi_1^\circ)}{2}\left[(\hat{\mathbf{b}}_\mathbf{1}\wedge\hat{\mathbf{K}}_\mathbf{1})\cdot\hat{\mathbf{K}}_\mathbf{2}\right]\left[(\hat{\mathbf{a}}_\mathbf{2}\wedge\hat{\mathbf{K}}_\mathbf{2})\cdot\hat{\mathbf{K}}_\mathbf{1}\right]\right. \\ &\quad\left.+\frac{r_v(\chi_1^\circ)}{2}(\hat{\mathbf{b}}_\mathbf{1}\cdot\hat{\mathbf{K}}_\mathbf{2})(\hat{\mathbf{a}}_\mathbf{2}\cdot\hat{\mathbf{K}}_\mathbf{1})\right\} \end{aligned} \quad (23)$$

and the polarization general term in transmission (for $s\equiv t$, implying $\mathbf{K_s}=\mathbf{K_3}$) $F_{t,\alpha\beta}(\mathbf{K_1},\mathbf{K_3})$ is defined by

$$\begin{aligned} &F_{t,\alpha\beta}(\mathbf{K_1},\mathbf{K_3}) \\ &\quad= \frac{2\|\hat{\mathbf{K}}_\mathbf{3}-k_\alpha/k_\beta\hat{\mathbf{K}}_\mathbf{1}\|\left(\hat{\mathbf{N}}^{\mathbf{0(t)}}\cdot\hat{\mathbf{K}}_\mathbf{3}\right)}{\|\hat{\mathbf{K}}_\mathbf{1}\wedge\hat{\mathbf{K}}_\mathbf{3}\|^2|\hat{k}_{3z}-k_\alpha/k_\beta\hat{k}_{1z}|} \\ &\quad\times\left\{\frac{t_h(\chi_1^\circ)}{2}\left[(\hat{\mathbf{b}}_\mathbf{1}\wedge\hat{\mathbf{K}}_\mathbf{1})\cdot\hat{\mathbf{K}}_\mathbf{3}\right]\left[(\hat{\mathbf{a}}_\mathbf{3}\wedge\hat{\mathbf{K}}_\mathbf{3})\cdot\hat{\mathbf{K}}_\mathbf{1}\right]\right. \\ &\quad\left.+\frac{t_v(\chi_1^\circ)}{2}(\hat{\mathbf{b}}_\mathbf{1}\cdot\hat{\mathbf{K}}_\mathbf{3})(\hat{\mathbf{a}}_\mathbf{3}\cdot\hat{\mathbf{K}}_\mathbf{1})\right\} \end{aligned} \quad (24)$$

with $\mathbf{K_1}$ the incident wave vector inside the medium Ω_α and $\mathbf{K_3}$ the scattered wave vector in transmission inside the medium Ω_β.

The contribution of the third-order NRCS $\bar{\sigma}_{r,3}$ is given by

$$\begin{aligned} &\bar{\sigma}_{r,3}(\mathbf{K_r},\mathbf{K_i}) \\ &\quad= \frac{1}{\cos\theta_i}\int \sin\theta_{m1}d\theta_{m1}d\phi_{m1}\sin\theta_{m2}d\theta_{m2}d\phi_{m2} \\ &\qquad\left|\bar{F}_{t,12}(\mathbf{K_i},\mathbf{K_{m1}})\times\bar{r}_{23}(\theta_{m1})\times\bar{F}_r(\mathbf{K_{p1}},\mathbf{K_{m2}})\right. \\ &\qquad\left.\times\bar{r}_{23}(\theta_{m2})\times\bar{F}_{t,21}(\mathbf{K_{p2}},\mathbf{K_r})\right|^2 \\ &\qquad\cdot\frac{p_s\left(\boldsymbol{\gamma}_{\mathbf{A_1}}^{\mathbf{0(t)}}\right)}{\left|\hat{k}_{m1z}-\frac{k_1}{k_2}\hat{k}_{iz}\right|^2}S_{12}\left(\mathbf{K_i},\mathbf{K_{m1}}|\boldsymbol{\gamma}_{\mathbf{A_1}}^{\mathbf{0(t)}}\right) \\ &\qquad\cdot\frac{p_s\left(\boldsymbol{\gamma}_{\mathbf{A_2}}^{\mathbf{0(r)}}\right)}{|\hat{k}_{m2z}-\hat{k}_{p1z}|^2}S_{22}\left(\mathbf{K_{p1}},\mathbf{K_{m2}}|\boldsymbol{\gamma}_{\mathbf{A_2}}^{\mathbf{0(r)}}\right) \\ &\qquad\cdot\frac{p_s\left(\boldsymbol{\gamma}_{\mathbf{A_3}}^{\mathbf{0(t)}}\right)}{\left|\hat{k}_{rz}-\frac{k_2}{k_1}\hat{k}_{p2z}\right|^2}S_{21}\left(\mathbf{K_{p2}},\mathbf{K_r}|\boldsymbol{\gamma}_{\mathbf{A_3}}^{\mathbf{0(t)}}\right) \end{aligned} \quad (25)$$

and so on for the higher orders.

B. Model Validity Domains and Properties

The validity domains of the model are similar to those in the 2D problem (with 1D surfaces): see [11, Sec. 2.C]. However, slight differences appear, as conditions #1 and #5 on the mean curvature radius R_{cA} hold here for both its x- and y- components, $R_{cA,x}$ and $R_{cA,y}$, respectively. The same remark holds for condition #2 on the rms slope σ_{sA}, which holds for both $\sigma_{sA,x}$ and $\sigma_{sA,y}$. Moreover, as we will see in the numerical results, the main difference with the 2D case holds for cross-polarizations, where the condition is more restrictive, of the order of $\{\sigma_{sA,x},\sigma_{sA,y}\}\lesssim 0.2$. Based on the iteration of the Kirchhoff

approximation to compute scattering interactions among the interfaces of the rough layer and the high frequency approximation, the overall approach has the validity domain of the Geometrical Optics Approximation. That is why this method is called the Geometric Optics Approximation for a rough layer and is denoted GOA.

One can notice that this asymptotic model, generalized to a 3D problem (with 2D surfaces), has the same general properties as for the 2D case (with 1D surfaces). Indeed, it is independent of the height statistics (when the anti-coincidental contribution can be neglected), as well as of the frequency or of the mean layer thickness (for lossless inner media). This was verified by making numerical results for different values of the mean layer thickness and the rough surface height rms. As for the 2D case, the model in itself, as based on the GOA, cannot deal with lossy media. Still, by using exactly the same approach as for the 2D case (see [10, Sec. 7]), taking lossy media into account does not raise any problem.

Some simulation results, not presented here, were used to validate the first-order contribution $\sigma_{r,1}^{tot} = \sigma_{r,1}$ (corresponding to the scattering in reflection from a single surface) by comparison with results of the literature [21]. In the next section, asymptotic model predictions of the first two order contributions of the NRCS $\sigma_{r,1}^{tot} = \sigma_{r,1}$ and $\sigma_{r,2}^{tot} = \sigma_{r,1} + \sigma_{r,2}$ are compared with a reference numerical method for validation.

IV. Numerical Results: Asymptotic Model Validation

A. Numerical Reference Method

A numerical method based on the method of moments was developed for the configuration of Fig. 1 with a perfectly conducting region 3 following previous implementations for non-layered, penetrable rough surfaces [22]–[24] and for objects in the presence of a penetrable rough surface [25]–[27]. The latter problem can be directly extended to the case of interest by replacing the penetrable object previously considered [25] with a perfectly conducting surface. Although the code was implemented to be able to incorporate rough lower boundaries, here only flat lower interfaces were of interest.

The method discretizes both the upper and lower interfaces, the former in terms of the vector induced electric and magnetic current densities, while only induced electric current densities are required on the lower interface. To allow direct comparisons with the asymptotic approach, the combined matrix equation for induced currents on both interfaces was solved by iterating on successive couplings between the interfaces (i.e., the "orders" of the asymptotic approach); the implementation is described in detail in [25]. This requires that algorithms be implemented for determining induced current densities on each interface individually given an exciting field consisting of contributions from the incident field as well as radiation from the current densities found at lower orders. Solutions for the upper interface currents were also performed iteratively, and the canonical grid method [22]–[27] was used to accelerate the required matrix-vector multiply operations. No acceleration of computations of the coupling between layers was performed, so that overall algorithm is order N^2 where N is the total number of unknowns on the upper interface. Improvements in efficiency would be possible if acceleration methods were adopted for this coupling.

Reduction of surface edge effects given finite surface size were achieved by using the "tapered" incident field described in [22], [23], as is common in rough surface scattering studies. A half power spot diameter of 5.6 wavelengths was used, and fields at surface edges were reduced by 54 dB. Comparisons of scattering from the upper surface with standard asymptotic theories was used to verify that this approach should provide reasonable results for co-pol scattering within approximately 70 degrees scattering angle. These comparisons also showed the tapered wave to increase cross-polarized scattered fields significantly above the very small cross-sections predicted by standard theories. However, the presence of the lower layer dramatically increases cross-pol results, so that reasonable predictions are apparently achieved for cross-polarization in the presence of the lower layer.

The results to be illustrated consider a layer of relative permittivity $\epsilon_{r2} = 3$, above a flat perfectly conducting boundary $(\epsilon_{r3} = i\infty)$. Surface sizes of 24 by 24 free space wavelengths were used, discretized into 256 by 256 points for a total of 393216 unknowns in the matrix equation (4 unknowns for each point on the upper interface, 2 on the lower). The upper surface profiles were generated as realizations of a Gaussian stochastic process with an isotropic Gaussian correlation function. Two roughness cases are considered: rms height 0.25λ and correlation length 1.768λ or rms height 0.3λ and correlation length 2.12λ. Both cases have rms slope 0.2. A distance of 2.41 free space wavelengths between the layers was used in the numerical method; simulations using other distances showed only a very weak dependence on this distance (likely due to tapered wave issues), consistent with the asymptotic method which predicts an independence of this distance. While the asymptotic method should be applicable for surfaces with even larger rms heights, the canonical grid method acceleration technique used in the numerical algorithm is best suited for moderate rms height surfaces. A total of thirty-two surface realizations (sufficient to achieve mean NRCS estimates accurate to within approximately 2 dB) were used in each simulation, with the required computations performed on parallel computing resources at the Maui High Performance Computing Center. The parallel computing algorithm was developed to use groups of 8 processors for a single surface realization, so that required couplings between the upper and lower interfaces could be computed more rapidly. Results for a single surface realization using eight processors were achieved in approximately 5 hours of CPU time. By comparison, the typical CPU time to compute the asymptotic GO method is of the order of 5 seconds on a standard personal computer using MATLAB.

In the comparisons to be shown, the incident wave is linearly polarized with an incident elevation angle θ_i of either 0 (normal incidence) or 15 degrees, and the incident azimuth angle is always $\phi_i = 0°$. The numerical results present the total NRCS in reflection $\sigma_{r,n}^{tot}$ for HH, HV, VH, VV polarizations (the first term representing the polarization of the scattered wave, and the second term the polarization of the incident wave) and in either the incident plane $(\phi_r = 0)$ or in scattering planes rotated azimuthally with respect to the plane of incidence (ϕ_r not zero).

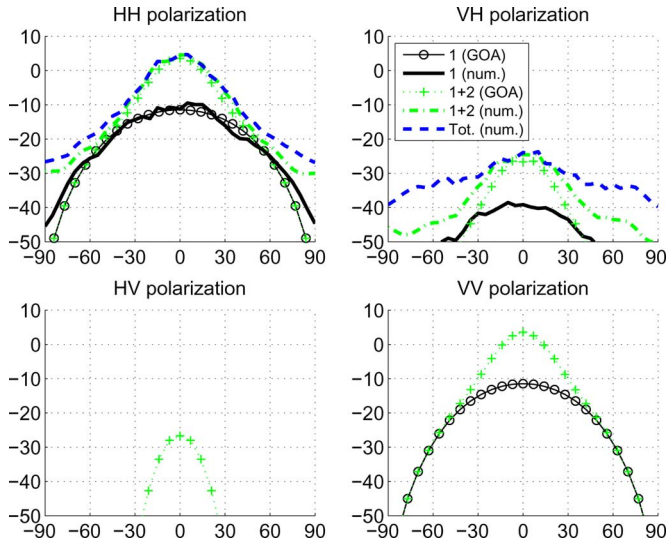

Fig. 2. Simulation of the first two total NRCSs $\sigma_{r,1}^{tot}$, and $\sigma_{r,2}^{tot}$ in dB scale, with respect to the observation angle θ_r in the plane of incidence (azimuth angle $\phi_r = 0°$), for an incidence elevation angle $\theta_i = 0°$.

B. Simulation Results

Fig. 2 presents numerical results for scattering in the plane of incidence (azimuth angle $\phi_r = 0°$) for an incidence angle $\theta_i = 0°$. For the GOA, the first-order contribution $\sigma_{r,1}^{tot} = \sigma_{r,1}$ with shadowing effects is plotted as a black line with circles (the case without shadowing effects is not presented as no difference appears). The second-order contribution $\sigma_{r,2}^{tot} = \sigma_{r,1} + \sigma_{r,2}$ with shadowing effects is plotted as a green dotted line with plus signs (the case without shadowing effects is not presented here for the sake of clarity of the figures). For the numerical simulations of the reference numerical method, results are presented in HH and VH polarizations only for this case, using surfaces of rms height 0.25λ and correlation length 1.768λ. The contribution from the upper interface alone obtained from the numerical method, corresponding to $\sigma_{r,1}^{tot} = \sigma_{r,1}$, is plotted as a black line. The result after one iteration of the method, corresponding to $\sigma_{r,2}^{tot} = \sigma_{r,1} + \sigma_{r,2}$, is plotted as a green dash-dot line, and the result after many iterations, corresponding to $\sigma_{r,n}^{tot} \simeq \sigma_{r,\infty}^{tot}$, is plotted as a blue dashed line.

In co-polarizations HH and VV, the two first-order contributions $\sigma_{r,1}^{tot}$ and $\sigma_{r,2}^{tot}$ of the GOA have the same basic properties as in the 2D problem (see [10, Sec. 6] and [11, Sec. 3.C]). The second-order NRCS $\sigma_{r,2}^{tot}$ contributes primarily around the specular direction, where the NRCS is much larger than that of the first-order contribution $\sigma_{r,1}^{tot}$. Similarly as for the 2D problem, the case without shadowing effects (which is not represented here for the sake of clarity of the figure) diverges for observation angles $|\theta_r| > 60°$: this highlights the relevance of taking shadowing into account. In cross-polarizations VH and HV, as expected by the first-order KA, the first-order NRCS $\sigma_{r,1}^{tot}$ of the GOA has a negligible contribution compared to the second-order contribution $\sigma_{r,2}^{tot}$.

For HH polarization, the comparison with the reference numerical method shows a very good agreement for $\sigma_{r,1}^{tot}$, which corresponds to the scattering from the upper surface when no lower layer is present. The differences that appear for grazing angles, $|\theta_r| \gtrsim 75°$, are likely impacted by the finite surface size as well as the limitations of the KA theory (more precisely, the neglect of the multiple scattering from the rough interface effect) for this region. Very good agreement is also observed for the second-order contribution $\sigma_{r,2}^{tot}$; significant differences are observed only for grazing angles, $|\theta_r| \gtrsim 60°$, also are likely impacted by the finite surface size as well as limitations of the GO theory. More complete numerical simulations would be required to clarify these differences. Nevertheless, the observed differences in co-polarizations are very similar to the ones obtained for a 2D problem: for instance, see [11, Fig 6] for a similar configuration. Thus, it is more likely that the GOA limitations, and in particular the neglect of multiple scattering effects, rather than the finite surface size of the numerical model, explains these differences. The result of the numerical method for many iterations highlights that around the specular direction for these surfaces, there is no significant difference with the first iteration $\sigma_{r,2}^{tot}$, which means that $\sigma_{r,2}^{tot}$ is sufficient to quantify the scattering process. This result is in agreement with observations made for a 2D problem (see [11, Sec 3.C]). Thus, in co-polarization, the second-order contribution $\sigma_{r,2}^{tot}$ of the GOA model can correctly quantify the scattering process around the specular direction, for observation angles $|\theta_r| \lesssim 60°$.

For cross-polarization VH, the comparison of the GOA with the reference method highlights a good agreement for the second-order contribution $\sigma_{r,2}^{tot}$ near the specular direction, $|\theta_r| \lesssim 20°$. The differences that appear for higher $|\theta_r|$ may be attributed to multiple scattering from the same interface effect or possibly to finite surface size effects, although such effects would likely not be major contributors for angles within 30 degrees scattering angle. The total scattering coefficient computed from the reference method shows larger contributions away from the specular direction. Thus, in cross-polarization, the second-order contribution $\sigma_{r,2}^{tot}$ of the GOA model appears sufficient for these statistics to describe the scattering process near the specular direction, for observation angles $|\theta_r| \lesssim 15°$. Note the low level first order (i.e. upper surface only with no interface) cross-polarization response obtained by the numerical reference method, which is likely an overestimate of the true value due to the impact of the tapered incidence field. However the much larger values for in-plane cross-polarized NRCS values in the presence of the layer reduces the impact of tapered wave effects.

Fig. 3 presents results for the same parameters as in Fig. 2, but for out-of-plane scattering at azimuth angle $\phi_r = 75°$. As $\phi_r = 75°$ is close to the quadrature angle $(= 90°)$, the numerical results for co-polarizations are rather similar to those for cross-polarization obtained in Fig. 2 and vice-versa. Therefore, co-pol and cross-pol results here can largely be interpreted in the same manner as used for cross-pol and co-pol results, respectively, in the in-plane scattering case. The main distinctions of such an approach appear in co-polarization: due to the difference of 15° with respect to a perpendicular scattering plane, the first-order contribution $\sigma_{r,1}^{tot}$ of the GOA cannot be neglected. Moreover, the second-order contribution $\sigma_{r,2}^{tot}$ increases and reaches approximately -7 dB in the specular direction $\theta_r = 0°$. The agreement of the GOA with the reference method is somewhat improved in this comparison compared to that for the plane-of-in-

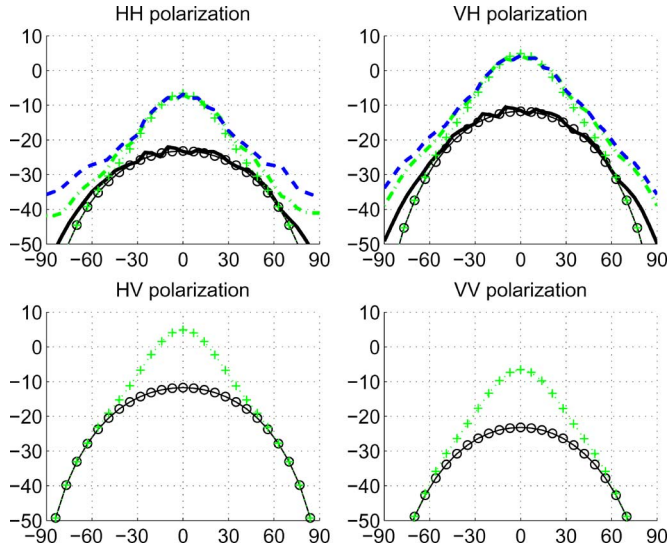

Fig. 3. Same simulations as in Fig. 2, but with an azimuth angle $\phi_r = 75°$.

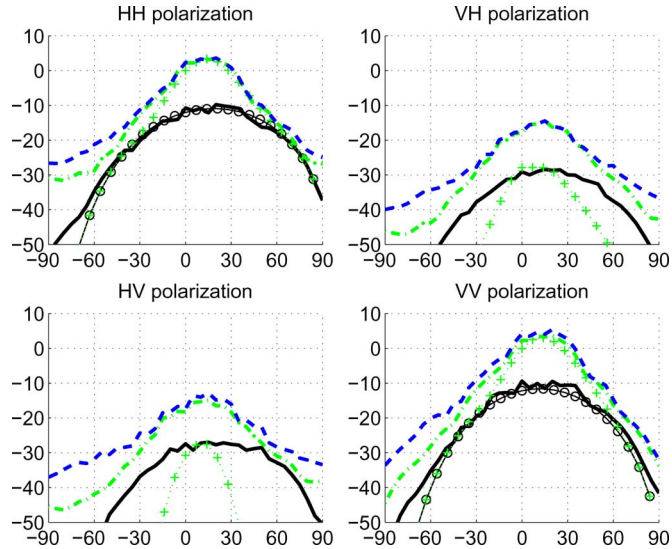

Fig. 4. Same simulations as in Fig. 2, but with an incidence elevation angle $\theta_i = 15°$.

cidence, since first-order scattering effects are more important in both polarizations, leading to a lower relative contribution of the multiple scattering effects.

Other comparisons (not presented here) for various rotations of the scattering plane (i.e. ϕ_r values) allowed a check on the symmetry of the NRCS of the GOA around $\phi_r = 90°$ and its 180°-periodicity (owing to the isotropy of the rough surface). For example, NRCS values for $\phi_r = 180°$ and $\phi_r = 360°$ are similar to those for $\phi_r = 0°$, and the results for $\phi_r = 105°$, $\phi_r = 220°$ and $\phi_r = 250°$ are similar to those for $\phi_r = 75°$. As the azimuth angle ϕ_r moves away from 0° or 90°, the lower polarization contribution (VH or HH, respectively) increases and shows an increasingly good agreement of the GOA with the reference method around and away from the specular direction.

Fig. 4 presents comparisons for the parameters of Fig. 2, but with an incidence angle $\theta_i = 15°$. While the upper surface RMS slope σ_s remains unchanged, the reference numerical method used a surface RMS height $\sigma_h = 0.3\lambda$, and $L_c = 2.12\lambda$. The results show the same general behavior of the GOA as in the preceding configuration. The results for the case without shadowing effects (not presented here for the sake of clarity of the figure) again diverge for grazing θ_r. The results of the GOA are compared with the reference numerical method for all polarizations (HH, VH, HV, VV). In co-polarizations HH and VV, the first-order contribution $\sigma_{r,1}^{tot}$ highlights a good agreement of the GOA with the reference method. Again differences that appear for larger θ_r values, and in particular for $\theta_r < 0$, can be attributed to the limitations of the GOA as well as tapered wave effects at the larger angles. The second-order contribution $\sigma_{r,2}^{tot}$ highlights a good agreement of the GOA with the reference method in and around the specular direction, and in HH polarization for θ_r up to approximately positive 80°. The differences that appear away from the specular direction, in particular for backward configuration $\theta_r < 0$, are likely primarily due to limitations of the GOA, owing to the neglect of the multiple scattering effect. As in Fig. 2, results from the reference numerical method highlight that in and around the specular direction, the higher orders are negligible: the second-order $\sigma_{r,2}^{tot}$ is enough to quantify the scattering phenomenon. A comparison (not presented here) between the in-plane co-polarized 3D results and the 2D results of the GOA model was made for the same roughness statistics and layer dielectric properties. The comparison showed that for the first-order contribution $\sigma_{r,1}$, the ratio $C_{r,1}$ of the 3D case to the 2D case is weak (less than 1 dB) for moderate incidence angles and moderate scattering angles. It can be shown that this ratio is given for a Gaussian height pdf and without shadowing effects by

$$C_{r,1} = \frac{1}{\cos\theta_r + \cos\theta_i} \times \frac{1}{\sigma_s\sqrt{2\pi}}. \tag{26}$$

Nevertheless, for the second-order contribution $\sigma_{r,2}$, the ratio cannot be expressed from a simple formula, and the difference is much more significant (of the order of 4 dB around the specular direction), and significantly varies at other angles.

In cross-polarizations VH and HV, as in Fig. 2, results from the GOA confirm that $\sigma_{r,1}^{tot}$ has a negligible contribution, while $\sigma_{r,2}^{tot}$ which has a moderate contribution around the specular direction. The reference method again shows appreciable contributions for $\sigma_{r,1}^{tot}$ that are impacted by the tapered wave and are likely to be overestimates of the true scattering. In contrast to Fig. 2 where a good agreement was found for second order cross-polarized NRCS values in and near around the specular direction, the GOA here underestimates cross-polarized scattering. This is likely due to the impact of multiple scattering on the upper interface, which plays a significant role generally in cross-polarized scattering. The results of the reference method for higher orders confirm that the second-order contribution when computed exactly yields sufficient accuracy for these surface statistics around the specular direction.

Fig. 5 presents numerical results for the same parameters as in Fig. 4, but for a rotated scattering plane at azimuth angle $\phi_r = 105°$. As for the first case, $\phi_r = 105°$ is close to the quadrature angle ($= 90°$), and an interchange of co- and cross-polarized results can be used to help interpret NRCS properties. The main

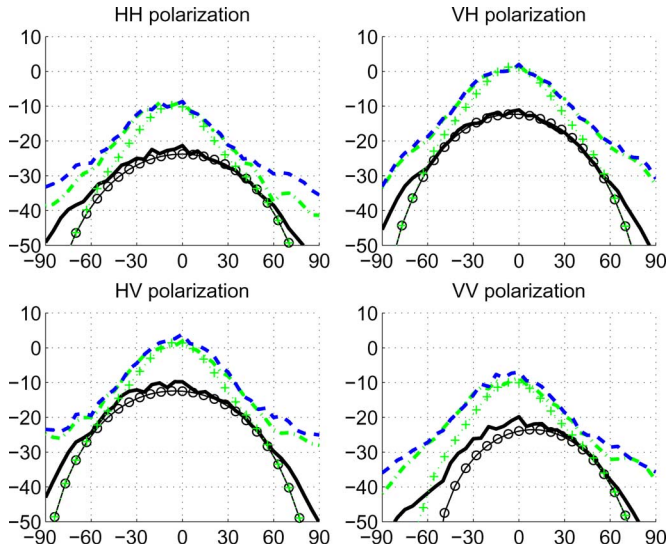

Fig. 5. Same simulations as in Fig. 4, but with an azimuth angle $\phi_r = 105°$.

distinctions from such an interchange appear in co-polarization, again since the first order contribution is appreciable for this geometry. Overall, a good agreement is found with the reference method because multiple scattering effects are less important when compared to first order scattering processes. Moreover, the second-order contribution $\sigma_{r,2}^{tot}$ of the GOA increases, so that the multiple scattering from the same interface effect has a less important relative contribution. Thus, there is a good agreement of the GOA with the reference method in and around the specular direction. Other comparisons (not presented here) for various values of ϕ_r provide similar conclusions. Overall, these comparisons validate the GOA in its validity domain, and help to quantify limitations of the approach for scattering angles away from the specular direction and for cross-polarized predictions in the plane of incidence at non-normal incidence angles.

V. Conclusion

In conclusion, the GOA for a rough layer has been extended to a general 3D problem with 2D surfaces, allowing it to model more realistic problems and to study the influence of cross-polarizations. Comparisons with a reference numerical method validated the GOA in its validity domain. The two different configurations used confirmed that the model is independent of the RMS surface height. Results showed that in and around the specular direction, the second-order contribution $\sigma_{r,2}^{tot}$ is sufficient to quantify the scattering process. Observed differences of the GOA with the reference method can be attributed primarily to multiple scattering effects on the upper interface.

References

[1] C. Moss, T. Grzegorczyk, H. Han, and J. Kong, "Forward-backward method with spectral acceleration for scattering from layered rough surfaces," *IEEE Trans. Antennas Propag.*, vol. 54, no. 10, pp. 2917–2929, 2006.

[2] N. Déchamps and C. Bourlier, "Electromagnetic scattering from a rough layer: Propagation-inside-layer expansion method combined to an updated BMIA/CAG approach," *IEEE Trans. Antennas Propag.*, vol. 55, no. 10, pp. 2790–2802, Oct. 2007.

[3] N. Déchamps and C. Bourlier, "Electromagnetic scattering from a rough layer: Propagation-inside-layer expansion method combined to the forward-backward novel spectral acceleration," *IEEE Trans. Antennas Propag.*, vol. 55, no. 12, pp. 3576–3586, Dec. 2007.

[4] I. Ohlídal and K. Navrátil, "Scattering of light from multilayer with rough boundaries," in *Progr. Opt.*, E. Wolf, Ed. : Elsevier Science, 1995, vol. XXXIV, pp. 248–331.

[5] Z.-H. Gu, I. Fuks, and M. Ciftan, "Grazing angle enhanced backscattering from a dielectric film on a reflecting metal substrate," *Opt. Eng.*, vol. 43, no. 3, pp. 559–567, 2004.

[6] A. Soubret, G. Berginc, and C. Bourrely, "Application of reduced Rayleigh equations to electromagnetic wave scattering by two-dimensional randomly rough surfaces," *Phys. Rev. B*, vol. 63, no. 24, p. 245411, Jun. 2001.

[7] E. Bahar and Y. Zhang, "Diffuse like and cross-polarized fields scattered from irregular layered structures-full-wave analysis," *IEEE Trans. Antennas Propag.*, vol. 47, no. 5, pp. 941–948, May 1999.

[8] A. Fung, *Microwave Scattering and Emission Models and Their Applications*. Boston, MA: Artech House, 1994.

[9] G. Berginc and C. Bourrely, "The small-slope approximation method applied to a three-dimensional slab with rough boundaries," *Progr. Electromagn. Res.*, vol. 73, pp. 131–211, 2007.

[10] N. Pinel, N. Déchamps, C. Bourlier, and J. Saillard, "Bistatic scattering from one-dimensional random rough homogeneous layers in the high-frequency limit with shadowing effect," *Waves in Random and Complex Media*, vol. 17, no. 3, pp. 283–303, Aug. 2007.

[11] N. Pinel and C. Bourlier, "Scattering from very rough layers under the geometric optics approximation: Further investigation," *J. Opt. Society Amer. A*, vol. 25, no. 6, pp. 1293–1306, Jun. 2008.

[12] C. Bourlier, G. Berginc, and J. Saillard, "Monostatic and bistatic statistical shadowing functions from a one-dimensional stationary randomly rough surface according to the observation length: I. Single scattering," *Waves Random Media*, vol. 12, no. 2, pp. 145–173, 2002.

[13] N. Pinel, C. Bourlier, and J. Saillard, "Energy conservation of the scattering from rough surfaces in the high-frequency limit," *Opt. Lett.*, vol. 30, no. 15, pp. 2007–2009, Aug. 2005.

[14] C. Bourlier, G. Berginc, and J. Saillard, "Bistatic scattering coefficient from one- and two-dimensional random surfaces using the stationary phase and scalar approximation with shadowing effect: Comparisons with experiments and application to the sea surface," *Waves Random Media*, vol. 11, no. 2, pp. 119–147, Apr. 2001.

[15] J. Stratton, *Electromagnetic Theory*. New York: McGraw-Hill, 1941.

[16] J. A. Kong, *Electromagnetic Wave Theory*, 2nd ed. New York: Wiley, 1990.

[17] F. Bass and I. Fuks, *Wave Scattering From Statistically Rough Surfaces*, C. B. Vesecky and J. F. Vesecky, Eds. Oxford, U.K.: Pergamon Press, 1978.

[18] C. Bourlier and G. Berginc, "Multiple scattering in the high-frequency limit with second-order shadowing function from 2D anisotropic rough dielectric surfaces: I. Theoretical study," *Waves Random Media*, vol. 14, no. 3, pp. 229–252, 2004.

[19] L. Tsang and J. Kong, *Scattering of Electromagnetic Waves, Volume III: Advanced Topics*. New York: Wiley, 2001.

[20] L. Tsang, E. Njoku, and J. Kong, "Microwave thermal emission from a stratified medium with nonuniform temperature distribution," *J. Appl. Phys.*, vol. 46, no. 12, pp. 5127–5133, 1975.

[21] C. Bourlier and G. Berginc, "Multiple scattering in the high-frequency limit with second-order shadowing function from 2D anisotropic rough dielectric surfaces: II. Comparison with numerical results," *Waves Random Media*, vol. 14, no. 3, pp. 253–276, 2004.

[22] K. Pak, L. Tsang, and J. T. Johnson, "Numerical simulations and backscattering enhancement of electromagnetic waves from two dimensional dielectric random rough surfaces with sparse matrix canonical grid method," *J. Opt. Society Amer. A*, vol. 14, no. 7, pp. 1515–1529, 1997.

[23] J. T. Johnson, R. T. Shin, J. A. Kong, L. Tsang, and K. Pak, "A numerical study of the composite surface model for ocean scattering," *IEEE Trans. Geosci. Remote Sensing*, vol. 36, no. 1, pp. 72–83, 1998.

[24] J. T. Johnson, R. T. Shin, J. A. Kong, L. Tsang, and K. Pak, "A numerical study of ocean polarimetric thermal emission," *IEEE Trans. Geosci. Remote Sensing*, vol. 37, no. 1, pt. I, pp. 8–20, 1999.

[25] J. T. Johnson and R. J. Burkholder, "Coupled canonical grid/discrete dipole approach for computing scattering from objects above or below a rough interface," *IEEE Trans. Geosci. Remote Sensing*, vol. 39, pp. 1214–1220, 2001.

[26] J. T. Johnson, "A numerical study of scattering from an object above a rough surface," *IEEE Trans. Antennas Propag.*, vol. 40, pp. 1361–1367, 2002.

[27] J. T. Johnson and R. J. Burkholder, "A study of scattering from an object below a rough interface," *IEEE Trans. Geosci. Remote Sensing*, vol. 42, pp. 59–66, 2004.

Nicolas Pinel (S'05–M'07) was born in Saint-Brieuc, France, in 1980. He received the Engineering degree and the M.S. degree in Electronics and Electrical Engineering from Ecole polytechnique de l'université de Nantes (EpuN), Nantes, France, in 2003 and the Ph.D. degree from the University of Nantes, France, in October 2006.

He is currently working in the Radar team of the Institut de Recherche en Electrotechnique et Electronique de Nantes Atlantique (IREENA Laboratory), Nantes, France, on asymptotic methods of electromagnetic wave scattering from stacks of rough interfaces, and its application to oil slicks on sea surfaces at moderate and grazing incidence angles.

Joel T. Johnson (S'88–M'96–SM'03–F'07) received the B.E.E. degree from the Georgia Institute of Technology, Atlanta, in 1991, and the S.M. and Ph.D. degrees from the Massachusetts Institute of Technology, Cambridge, in 1993 and 1996, respectively.

He is currently a Professor in the Department of Electrical and Computer Engineering and ElectroScience Laboratory, The Ohio State University, Columbus. His research interests are in the areas of microwave remote sensing, propagation, and electromagnetic wave theory.

Dr. Johnson received the 1993 Best Paper Award from the IEEE Geoscience and Remote Sensing Society, was named an Office of Naval Research Young Investigator, National Science Foundation Career awardee, and Presidential Early Career Award for Scientists and Engineers award recipient in 1997, and was recognized by the U.S. National Committee of Union of Radio Science (URSI) as a Booker Fellow in 2002. He is a member of commissions B and F of the International URSI, and a member of Tau Beta Pi, Eta Kappa Nu, and Phi Kappa Phi.

Christophe Bourlier (A'99) was born in La Flèche, France, on July 6, 1971. He received the M. S. degree in electronics from the University of Rennes, Rennes, France, in 1995 and the Ph.D. degree from the Système Electronique et Informatique Laboratory (SEI), University of Nantes, Nantes, France, in 1999.

While at the University of Rennes, he was with the Laboratory of Radiocommunication where he worked on antennas coupling in the VHF-HF band. Now, he is with Institut de Recherche en Electrotechnique et Electronique de Nantes Atlantique (IREENA Laboratory), Nantes, France, in the Radar team at Polytech'Nantes (University of Nantes, France). He works as an Assistant Researcher of National Center for Scientific Research on electromagnetic wave scattering from rough surfaces and objects for remote sensing applications. He is author of more than 90 journal articles and conference papers.